Critical-angle transmission grating technology development for high resolving power soft x-ray spectrometers on Arcus and Lynx

Ralf K. Heilmann,[1] Alexander R. Bruccoleri,[2] Jungki Song,[1] Jeffery Kolodziejczak,[3] Jessica A. Gaskin,[3] Stephen L. O'Dell,[3] Peter Cheimetz,[4], Edward Hertz,[4] Randall K. Smith,[4] Vadim Burwitz,[5] Gisela Hartner,[5] Marlis-Madeleine La Caria,[5] and Mark L. Schattenburg,[1]

[1]Space Nanotechnology Laboratory, MIT Kavli Institute for Astrophysics and Space Research, Massachusetts Institute of Technology, Cambridge, Massachusetts 02139, USA
[2]Izentis LLC, PO Box 397002, Cambridge, MA 02139, USA
[3]NASA Marshall Space Flight Center, Huntsville, AL 35812, USA
[4]Center for Astrophysics, Harvard-Smithsonian Astrophysical Observatory, Cambridge, MA 02138, USA
[5]Max-Planck-Institut für Extraterrestrische Physik, 85748 Garching, Germany

ABSTRACT

Soft x-ray spectroscopy with high resolving power ($R = \lambda/\Delta\lambda$) and large effective area (A) addresses numerous unanswered science questions about the physical laws that lead to the structure of our universe. In the soft x-ray band $R > 1000$ can currently only be achieved with diffraction grating-based spectroscopy. Critical-angle transmission (CAT) gratings combine the advantages of blazed reflection gratings (high efficiency, use of higher diffraction orders) with those of conventional transmission gratings (relaxed alignment tolerances and temperature requirements, transparent at higher energies, low mass), resulting in minimal mission resource requirements, while greatly improving figures of merit. Diffraction efficiency $> 33\%$ and $R > 10,000$ have been demonstrated for CAT gratings. Last year the technology has been certified at Technology Readiness Level 4 based on a probe class mission concept. The Explorer-scale ($A > 450$ cm^2, $R > 2500$) grating spectroscopy Arcus mission can be built with today's CAT grating technology and has been selected in the current Explorer round for a Phase A concept study. Its figure of merit for the detection of weak absorption lines will be an order of magnitude larger than current instruments on Chandra and XMM-Newton. Further CAT grating technology development and improvements in the angular resolution of x-ray optics can provide another order of magnitude improvement in performance, as is envisioned for the X-ray Surveyor/Lynx mission concept currently under development for input into the 2020 Decadal Survey. For Arcus we have tested CAT gratings in a spectrometer setup in combination with silicon pore optics (SPO) and obtained resolving power results that exceed Arcus requirements before and after environmental testing of the gratings. We have recently fabricated the largest (32 mm x 32 mm) CAT gratings to date, and plan to increase grating size further. We mounted two of these large gratings to frames and aligned them in the roll direction using a laser-based technique. Simultaneous x-ray illumination of both gratings with an SPO module demonstrated that we can exceed Arcus grating-to-grating alignment requirements without x rays.

Keywords: critical-angle transmission grating, x-ray spectroscopy, blazed transmission grating, soft x-ray, grating spectrometer, high resolving power, Arcus, Lynx

1. INTRODUCTION

Soft x-ray spectroscopy of astrophysical sources is key to gaining a quantitative understanding of the history, dynamics, and current conditions of the cosmos. Ubiquitous plasmas emit and absorb at characteristic wavelengths

Further author information: Send correspondence to R.K.H. E-mail: ralf@space.mit.edu, URL: http://snl.mit.edu/home/ralf

Optics for EUV, X-Ray, and Gamma-Ray Astronomy VIII, edited by Stephen L. O'Dell, Giovanni Pareschi, Proc. of SPIE Vol. 10399, 1039914 · © 2017 SPIE · CCC code: 0277-786X/17/$18 · doi: 10.1117/12.2273000

and line intensity ratios that allow us to diagnose and map the physical conditions throughout our universe across a vast range of length scales and densities from the Cosmic Web to the atmospheres of stars. Examples are studies of the Warm Hot Intergalactic Medium, the search for the missing baryons, the study of the outflows of supermassive black holes, the properties of galaxy halos, and the effects of rotation, magnetic fields and stellar winds in stellar coronae.[1]

Several of these high-priority science questions were identified in the "New Worlds New Horizons" (NWNH) Astronomy and Astrophysics Decadal Survey,[2] as well as in the 2013 "Enduring Quests, Daring Visions" visionary Astrophysics Roadmap.[3]

The High Energy Transmission Grating Spectrometer (HETGS)[4] on Chandra and the Reflection Grating Spectrometer (RGS)[5] on XMM-Newton have revolutionized x-ray spectroscopy of celestial sources, but both missions were launched eighteen years ago with decades-old technology. They often can at best provide tantalizing hints of spectral features that require significantly higher resolving power R and effective area A.

The transmission grating geometry is very alignment insensitive and can preserve the exquisite 0.5 arcsec angular resolution of the Chandra mirrors with relaxed alignment tolerances, which results in R $\sim$ 1000 in the first diffraction orders. The RGS achieves much lower R, but has higher diffraction efficiency in the soft x-ray band due to its sawtooth groove profile that blazes efficiently at grazing angles of incidence below the critical angle for total external reflection. However, alignment tolerances and surface flatness requirements are significantly more challenging if reflection gratings are not to degrade the angular resolution of Chandra-like mirrors. In addition, the reflection grating surface area required to cover a given telescope aperture A_t is about $A_t/sin(\theta)$, with θ being the grazing angle of incidence on the order of 1-2 degrees. Transmission gratings operate at angles near normal incidence and therefore the required area is $\sim A_t$. For the same reasons transmission grating arrays have much lower mass than equivalent arrays of reflection gratings.

The advantages of the transmission geometry and the high efficiency of blazed gratings can be combined in a design called critical-angle transmission (CAT) grating. We have demonstrated CAT grating technology at Technology Readiness Level (TRL) 4,[6] with diffraction efficiency up to 33% and $R > 10,000$.[7] Further design improvements are expected to increase efficiency above 50%.

The Arcus[8,9] soft x-ray spectroscopy mission ($A > 450$ cm^2, $R > 2500$) has been selected together with two other submissions to the current NASA Midsize Explorer (MidEx) round for a Phase A concept study. Arcus is based on CAT grating technology in combination with silicon pore optics (SPOs)[10] as imaging optics and x-ray CCDs as readouts for the grating spectra. Today's CAT gratings already meet or exceed the Arcus requirements.

Lynx, formerly the X-ray Surveyor, is a mission concept to be submitted for input into the next Decadal Survey.[11,12] Science cases currently being formulated for Lynx call - among other performance requirements - for high-resolution soft x-ray spectroscopy with $A \sim 4000$ cm^2 and $R > 5,000$. Using the also envisioned 0.5 arcsec x-ray telescope angular resolution, this performance could be very reasonably achieved with CAT grating technology.

In the following we give a brief overview of the CAT grating principle and the grating fabrication progress and improvements to enable $\sim 32 \times 32$ mm^2 and presumably larger gratings. We then describe our recent measurements of resolving power of CAT gratings illuminated by an SPO module and diffraction efficiency before and after environmental testing, efficiency mapping of large gratings, laser-based roll alignment of gratings, and simultaneous x-ray illumination of two large aligned gratings.

2. CAT GRATING PRINCIPLE

Critical-angle transmission (CAT) gratings are freestanding transmission gratings with ultra-high aspect-ratio grating bars. They can be described as blazed transmission gratings and combine the advantages of past-generation transmission and blazed reflection gratings.[13–16] The basic structure of a CAT grating is shown in Fig. 1 in cross section. X rays are incident onto the sub-nm-smooth side walls of thin, ultra-high aspect-ratio grating bars at an angle α below the critical angle for total external reflection, θ_c (e.g., $\theta_c = 1.7°$ for 1 keV photons reflecting off a silicon surface). For optimum efficiency the grating depth d should be close to $a/\tan\alpha$ (a being the spacing between two adjacent grating bars), the grating bar thickness b should be as small as possible,

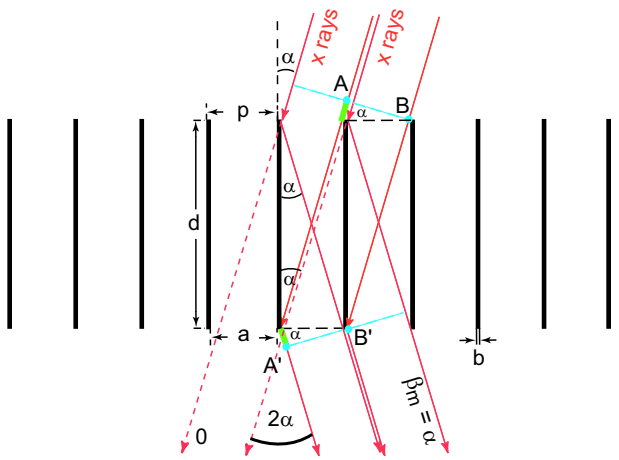

Figure 1. Schematic cross section through a CAT grating of period p. The m^{th} diffraction order occurs at an angle β_m where the path length difference between AA' and BB' is $m\lambda$. Shown is the case where β_m coincides with the direction of specular reflection from the grating bar side walls ($\beta_m = \alpha$), i.e., blazing in the m^{th}order.

and the gratings should be freestanding. As with any transmission grating, diffraction orders m appear at angles β_m given by the grating equation

$$\frac{m\lambda}{p} = \sin\alpha - \sin\beta_m, \tag{1}$$

with $m = 0, \pm1, \pm2, ...$, λ the x-ray wavelength, and p the grating period. Diffraction orders within a certain angular range around the direction of specular reflection off the sidewalls have enhanced efficiency ("blazing"), as long as $\alpha < \theta_c(\lambda)$.

3. CAT GRATING FABRICATION

We fabricate CAT gratings from <110> silicon-on-insulator (SOI) wafers. The grating bar mask is patterned using interference lithography, with the grating bars aligned parallel to the vertical silicon {111} planes. The CAT gratings and an integrated cross-support mesh (Level 1 or L1 supports) are etched out of the device layer or front side ($\sim$ 4 micron deep) using deep reactive-ion etching (DRIE). The device layer thickness determines the depth of the grating. We use the 500 μm thick SOI handle layer (back side) to separately etch out a high-throughput hexagonal Level 2 (L2) mesh that gives the thin device layer the necessary mechanical strength for a large-area membrane. Front and back side are separated by a 500 nm thick buried oxide (BOX) layer that serves as an etch stop. Fig. 2 gives a schematic representation of the structural hierarchy.

The etched front side is protected with photoresist and bonded to a carrier during the back side DRIE. After the backside etch the front side is wet-etched in KOH solution, polishing the rough grating bar sidewalls using the {111} planes as quasi-etch stops. In the end a vapor HF etch removes the BOX in the areas between the L2 supports, creating freestanding gratings. More detailed descriptions can be found elsewhere.[17–24] During the last year improvements in the process have enabled gratings spanning 32 x 32 mm^2, a threefold increase over the previous 32 x 10 mm^2 size. In the past process, AZ Electronic Materials 4620 photoresist was used to fill and protect the CAT grating bars bonded to a carrier during the back side etch. This etch worked on samples 32 x 10 mm^2 in size, but would overheat and destroy larger samples. The photoresist and bonding agent, Crystalbond 555, appeared to react adversely upon visual inspection of the bonds. The nature of the reaction was not clear, but voids were visible after de-bonds of partial etches. Photoresist was replaced with Brewer Science ProTEK SR-25, which both eliminated adverse reactions with Crystalbond and improved mechanical strength. ProTEK SR-25 is a material engineered to protect microstructures, and grating quality and yield were improved by using it. The backside DRIE step is also exothermic, and the etch tool uses a cooled chuck

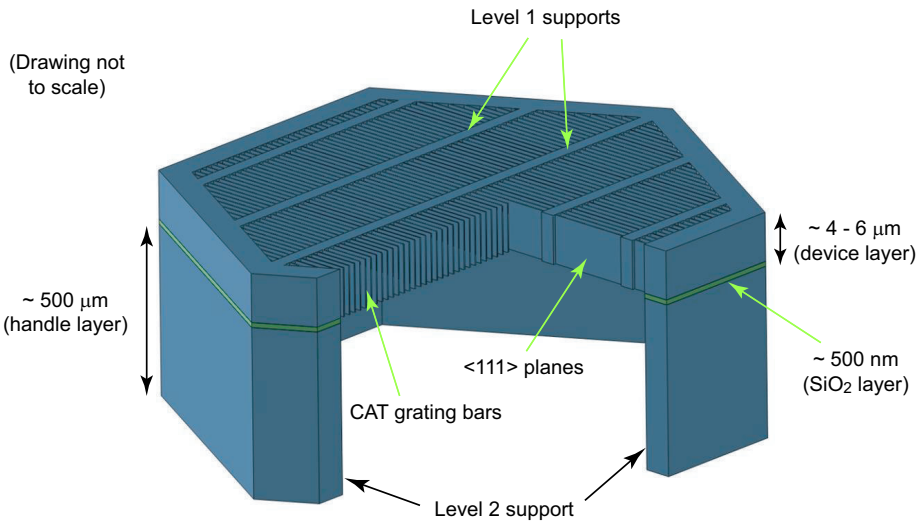

Figure 2. Schematic of a grating membrane "unit cell" (not to scale), formed by a single L2 support mesh hexagon. The L2 mesh is etched out of the SOI handle layer (back side). The device layer contains the fine-period CAT grating bars and in the perpendicular direction the coarse, low duty cycle integrated L1 support mesh. Device and handle layers are separated by the thin buried silicon oxide layer that serves as an etch stop for both front and back side etches.

to maintain the temperature of the sample. The etch can be sufficiently aggressive to overwhelm the cooling capacity of the chuck, and therefore the surface temperature of the silicon is a function of the open area being etched. As a result different recipes are required for the etching of 32 x 10 mm^2 and 32 x 32 mm^2 gratings. The durations of the etch and passivation steps of the backside etch were reduced to decrease the temperature of the etch, enabling consistent etches of 32 x 32 mm^2 gratings.

4. ARCUS CAT GRATING SPECTROMETER OPTICAL DESIGN

The Arcus optical design follows the tilted Rowland torus design,[25] described in more detail elsewhere.[26] The basic elements are shown in Fig. 3, consisting of a 12 m focal length x-ray telescope, an objective grating array, and a spectral readout. An azimuthal subsection of a full Wolter-I optic ("petal") is populated with SPO modules that focus x rays from infinity to a common focus. Using only an azimuthal subsection of a full Wolter optic produces an anisotropic point spread function (PSF) that is broad in the plane of reflection and narrow in the orthogonal direction (the so-called sub-aperture effect).[27] The petal is covered with an array of CAT gratings with their dispersion axes aligned along the narrow PSF axis, thus taking maximum advantage of the PSF anisotropy. The gratings are tangential to the surface of a Rowland torus that also contains the telescope focus and the readout array centered around the grating blaze peak. A second petal with gratings is placed symmetrically on the other side of the telescope optical axis and shares the same readout. Arcus uses a second pair of petals (B) with gratings with its optical axis shifted parallel to the first pair (A), and with its focus near the center of the first pair's blaze peak. This way the A-side readout detects the B-side's 0^{th} order image (plus nearby non-blazed, low-order diffraction peaks), and vice versa. This design allows for a compact utilization of the spacecraft aperture for effective area and simultaneous exploitation of the resolving-power-enhancing sub-aperture effect.

5. RESOLVING POWER MEASUREMENT OF A PROTOTYPE SPO-CAT GRATING SPECTROMETER

Last fall we performed measurements of the first 12 m focal-length SPO-based x-ray optical unit (XOU-0038), consisting of two aligned stacks of 21 uncoated silicon plates (65.7 mm wide in the azimuthal direction, 16.3 mm in the radial direction, 65% geometric open area, 737 mm nominal radius of curvature),[10] illuminating one of four $\sim 10 \times 30$ mm^2 CAT gratings (designated X1, X4, X7, and X9), at the Marshall Space Flight Center

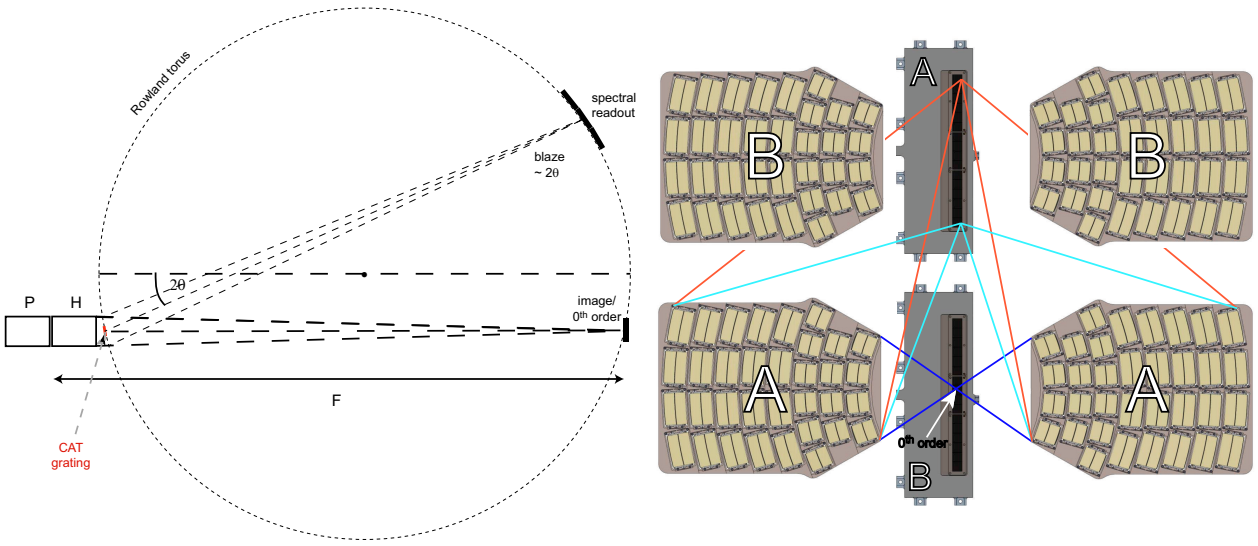

Figure 3. Left: Schematic of tilted Rowland torus optical design (not to scale). The source (far away to the left, not shown) is imaged via reflection from Wolter-I parabolic and hyperbolic mirror segments as the 0^{th} order on the right. CAT gratings with their normal inclined by an angle θ relative to the focused x rays blaze (enhance) the diffracted orders that fall onto the spectral readout. Our x-ray tests follow the same layout. Right: View from the source towards the image for the Arcus design. SPO XOUs in petal pair A image the source onto readout B (dark blue rays). The CAT grating arrays just downstream of the petals (not visible) generate diffracted orders. The strongest orders lie around the blaze angle and are focused onto readout A (light blue and red rays). The layout is mirror-symmetric around the plane between petal pairs A and B. The optical axis for the B petals is parallel to the A petal optical axis, but shifted upwards to fall onto readout A. CAT gratings behind the B petals blaze downwards onto readout B.

(MSFC) Stray Light Facility (SLF). The SLF features an electron bombardment source on one end of a 92 m beam line, and a 12 m long chamber on the other end with mounting stages for focusing optics and gratings, and an Andor CCD x-ray detector (13.5 μm pixel size) with vertical, horizontal, and focus translation at the far end of the chamber.

The XOU node was placed 87.8 m from the source in the 6 m long tapered section upstream of the large chamber and $f = 13.884$ m upstream of the detector due to the finite source distance. The XOU was oriented in the "parenthesis" orientation, meaning the optical axis of the XOU and the center of the XOU were in the same horizontal plane. Therefore the anisotropic point spread function of the XOU was oriented with its long axis in the horizontal direction and its short axis in the vertical direction (see Fig. 4). An optic aperture plate was used to select the azimuthally central 68% of the area of the XOU. Each grating was mounted over a 30×6 mm^2 hole on a plate, placed $d_{CAT-XOU} \sim 2,004$ mm from the optic node, with another movable 30×10 mm^2 aperture 150 mm upstream of the gratings. The gratings were oriented with their dispersion axes nominally in the vertical direction. One grating at a time was selected for illumination using linear translation stages. There was an empty 30×6 mm^2 slot in the grating plate for measurements of the direct beam. Illuminating the empty slot with the XOU we found a full width half max (FWHM) of 1.93" at best focus for the 1-D line spread function (LSF) projected onto the dispersion axis. If we subtract the estimated contribution to the width from the ~ 0.5 mm source size we obtain a FWHM of 1.6". The Arcus requirement for a full XOU is 2.0" FWHM.

The setup for these tests was primarily designed to measure diffraction from off-plane reflection gratings (OPGs).[28] Due to the different diffraction geometry for OPGs the angular range for the transmission grating geometry was limited to ~ 2.3 degrees, corresponding to 9^{th} order Al-K$_{\alpha 1,2}$ and 8^{th} order Mg-K$_{\alpha 1,2}$ characteristic lines, at diffraction angles of ~ 2.15 and 2.27 degrees from 0^{th} order, respectively. The design for Arcus is optimized for orders near 3.8 degrees, and has the gratings closer to the 12 m focal-length optics. For the SLF tests, if resolving power is only limited by the FWHM w of the LSF of the XOU, one can expect

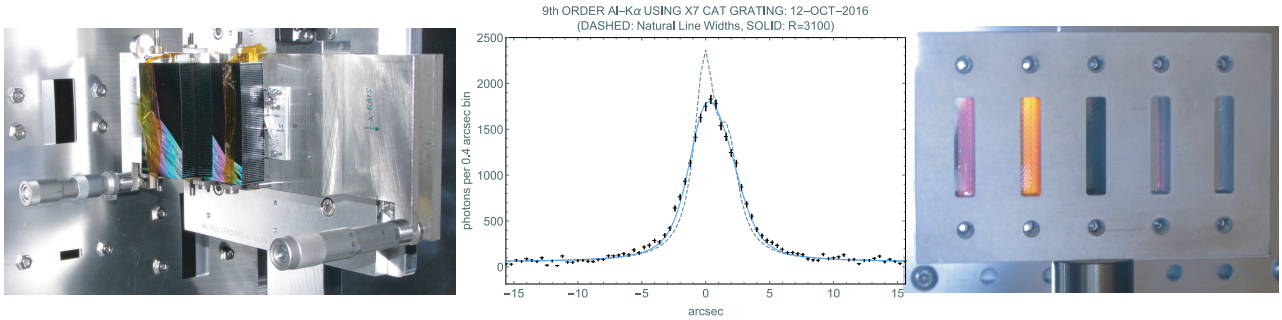

Figure 4. Left: SPO XOU-0038 mounted inside the SLF. X rays are incident from the left. The H stack consists of 21 plates, while the P stack has 34 plates. Only P plates that are followed by H plates are illuminated through the aperture visible at the left. Middle: 9^{th} order Al K_α diffraction peak from grating X7, projected onto the detector vertical axis, which is presumably parallel to the grating dispersion axis. The dashed line shows the $\alpha_{1,2}$ doublet based on the lines' natural widths. The data corresponds to a resolving power of $R \approx 3100$. Right: Upstream view of the grating plate, holding gratings X1, X4, X7, and X9. One hole is left open for calibration purposes.

$R \sim (\sin\beta'_m/w)(f - d_{CAT-XOU})/f$, with β'_m being the diffraction angle of the m^{th} order relative to 0^{th} order. The terms involving f take into account that the distance from the gratings to the detector is shorter than f. To estimate the actual resolving power we model the source spectrum using literature values for the natural widths and spacings of the K_α doublets[29] and fit the data by convolution of the diffracted theoretical spectrum with a Gaussian with variable width to obtain the FWHM.

Gratings X1 and X4 were conformally covered with nominally 7 nm of platinum on top of 2 nm of aluminum oxide using atomic layer deposition (ALD),[7] while X7 and X9 were plain silicon. We measured the diffraction efficiency of all four gratings at beam line 6.3.2 of the Advanced Light Source (ALS) synchrotron at Lawrence Berkeley National Laboratory (LBNL). Before x-ray testing at the SLF, gratings X7 and X9 had been epoxied at four points to titanium flexure frames[9] in order to facilitate later environmental testing and to gain experience with the bonding of CAT gratings to frames. Most of the available beam time was spent on samples X4, X7, and X9. We obtained resolving powers of 3100 for X4 and X7 (9^{th} order Al-K, see Fig. 4) and 2600 for X9 (8^{th} order Mg-K). Extrapolated to the Arcus design these numbers correspond to $R \sim 6200$ and 5000, respectively. Removing the estimated finite source size contribution leads to $R \sim 7200$ and 5400, respectively, and further improvements in the SPO LSF would lead to further increases in R. The expected Arcus resolving power will be smaller, however, since the SLF tests used a single XOU (utilized azimuthal extent = 2.3 deg) and benefit from the resulting strong sub-aperturing effect that narrows the LSF in the grating dispersion direction.[7,27] Arcus will use optics petals populated with many co-aligned XOUs, broadening the azimuthal extent to a range of up to $\sim \pm 25$ degrees and thus reducing the sub-aperture benefit to some degree.

6. ENVIRONMENTAL TESTING OF CAT GRATINGS

Gratings X7 and X9 underwent environmental testing at SAO after the above x-ray measurements. Both gratings were cycled six times under vacuum between -30 °C and +35 °C, with a ramp of 1 °C/minute and a dwell time of 15 minutes at each peak of the cycle. X9 was also vibration tested, shaking it along each axis at the following levels: 1.38 g's RMS - hold for 30 seconds; 2.77 g's RMS - hold for 30 seconds; 5.53 g's RMS (16.63 g's peak) - hold for 60 seconds. Visible inspection showed no changes or damage to the gratings. SEM imaging of X7 also did not show any damage to the grating structure (see Fig. 5).

7. RESOLVING POWER AFTER ENVIRONMENTAL TESTING

We repeated resolving power measurements of gratings X4, X7,and X9 with the same setup as in Section 5, and initially found reduced R for X7 and X9. Unfortunately, our measurements had been complicated by the fact that X7 and X9 had inadvertently been mounted with the device layer facing the detector instead of the source, as had been the case for the initial tests. We found post-experiment that this face reversal led to what appeared

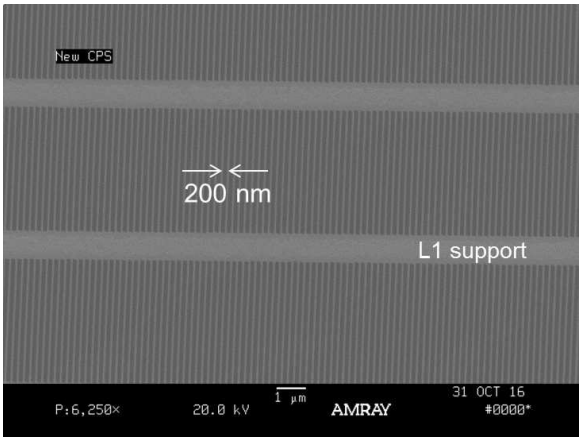

Figure 5. Top-down scanning electron micrograph of grating X7 after thermal cycling, showing undamaged 200 nm-period CAT grating bars and L1 cross supports.

to be a loss of resolving power, but was simply the effect of increased rotational misalignment between the L1 support mesh and the anisotropic optic PSF. The L1 supports act as a weak grating that nominally diffracts in the direction perpendicular to the CAT grating dispersion (the cross-dispersion) direction. This creates a rectangular diffraction pattern where every diffraction spot can be indexed as (m, n), where m is the diffraction order for the CAT grating bars, and n is the diffraction order for the L1 mesh. Typically the $n = 0$ orders are much stronger than the $n = \pm 1$ orders, with efficiencies for higher n orders falling off rapidly.

Ideally the L1 dispersion axis is aligned with the plane of reflection for the SPO plates, which is also the direction of the long axis of the anisotropic XOU point spread function (PSF). In that case L1 diffraction will be "smeared out" by the PSF and not lead to broadening in the CAT grating dispersion direction. However, if L1 diffraction is misaligned relative to the ideal orientation by some angle ϵ, potential for broadening and reduced resolving power exists.

The angle between CAT grating bars and L1 bars is set during two separate lithography steps. While this angle could be controlled to high precision, it currently is only controlled to the level of $\sim 1 - 2$ deg. Extensive post-campaign data analysis showed that the "flipping" of gratings X7 and X9 around the dispersion axis resulted in a rotation of the L1 dispersion axis in the laboratory frame of ~ 2.4 and 1.5 deg, respectively. During initial measurements both gratings had $|\epsilon| \sim 0.5$ deg, while after flipping we found $\epsilon \sim 1.9 - 2.0$ deg. (For X4, which was not moved, we found $\epsilon \sim 0.5$ deg before and ~ 0.6 deg after, compatible with no movement.) Misaligned cross-dispersion orders add Lorenztian-like wings to the LSF. Simple fits using single Gaussians therefore resulted in larger FWHM and presumably reduced values for R compared to the first round of tests. We separated out the effects of non-zero ϵ in two ways: A - We only used photons near the center of the XOU PSF, effectively removing cross-dispersed photons. B - We used the direct beam PSF to deconvolve the 0^{th} order image, remove the cross-dispersed orders, and predict the resolving power from the derived (0,0) order LSF (see Fig. 6). In both cases we found $R = 3000 - 3400$ for X7 and X9, both before and after environmental testing, and no indication of a reduction in R.

8. DIFFRACTION EFFICIENCY AFTER ENVIRONMENTAL TESTING

We again performed our x-ray diffraction efficiency measurements at beam line 6.3.2 of the ALS. The monochromatic x-ray beam is small enough to be centered inside an L2 hexagon without impinging on the L2 mesh. Diffraction efficiencies presented here are simply diode current from a slit-covered detector integrating over a single diffraction order, divided by diode current of the unobstructed direct beam. Since the beam size is more than fifty times larger than the L1 mesh period, absorption by the L1 mesh is included in the measurement.

We remeasured diffraction efficiency of X7 and X9 six months after initial efficiency measurements, which was seven weeks after the post-environmental-testing resolving power measurements. As seen in Fig. 7 we found no

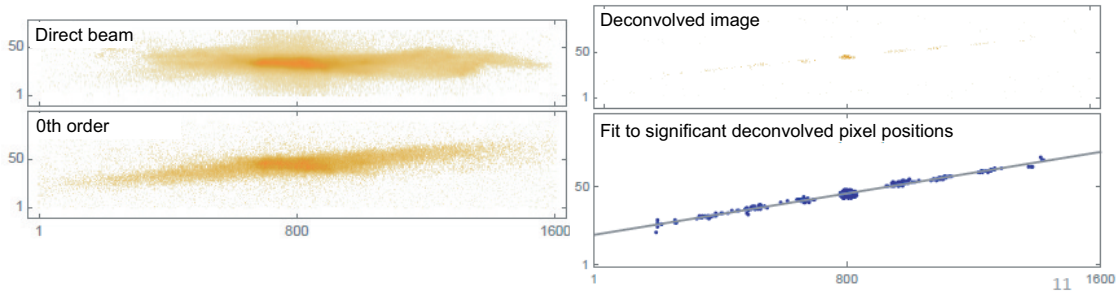

Figure 6. Left, top: Raw image of the direct beam from the XOU through the empty aperture in the grating plate. The long axis of the anisotropic PSF is approximately parallel to the horizontal detector axis (pixel rows). Left, bottom: Same detector position, but with grating X7 inserted, i.e. 0^{th} order image. The tails of the distribution appear tilted, which is due to the L1 dispersion direction not being parallel to the horizontal detector axis. Right, top: 0th order image, deconvolved with the direct beam PSF. The weak L1 diffraction peaks are visible. Right, bottom: Pixels with counts above a certain threshold, fit to a straight line, to deduce the angle of the L1 dispersion axis. (Note the different scaling for pixel rows and columns.)

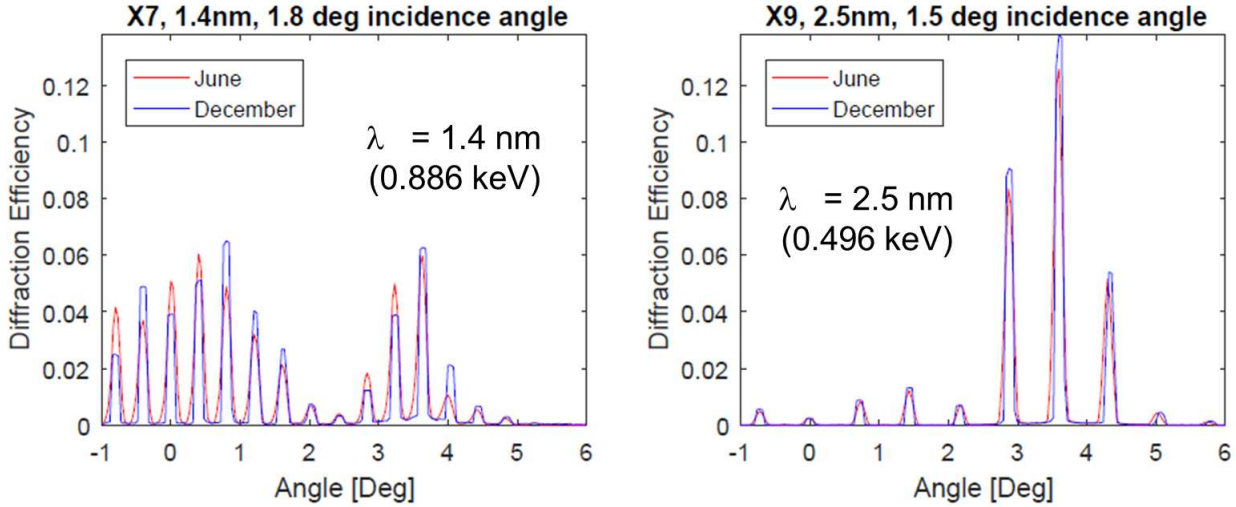

Figure 7. Representative examples of diffraction efficiency before (June) and after (Dec.) environmental testing for gratings X7 and X9 at two different wavelengths and incidence angles. Minor differences may be due to differences in synchrotron beam size (or apertures used) and placement on the samples, as well as small differences in incidence angles.

meaningful differences in diffraction efficiency between the two measurements, demonstrating that CAT gratings survive environmental testing and long periods of time without noticeable loss of efficiency.

9. FABRICATION OF 32×32 MM^2 CAT GRATINGS

Since the fabrication improvements described in Section 3 were put in place six 4 μm-deep large CAT gratings were fabricated with 86% yield. These gratings are large enough for each to cover more than half of an Arcus XOU. See Fig. 8 for an example.

10. DIFFRACTION EFFICIENCY OF LARGE CAT GRATINGS

We measured the diffraction efficiency of the first large grating (X10) at the ALS across a range of soft x-ray energies and found diffraction efficiencies as good as or slightly better than our previous records. The diffraction efficiency was mapped across the whole surface by raster-scanning the sample through the beam. Fig. 9 shows on the left the sum of efficiencies of the orders under the blaze envelope as a function of wavelength for a single spot on the grating, and on the right for 2.5 nm wavelength photons across the whole grating. The efficiency

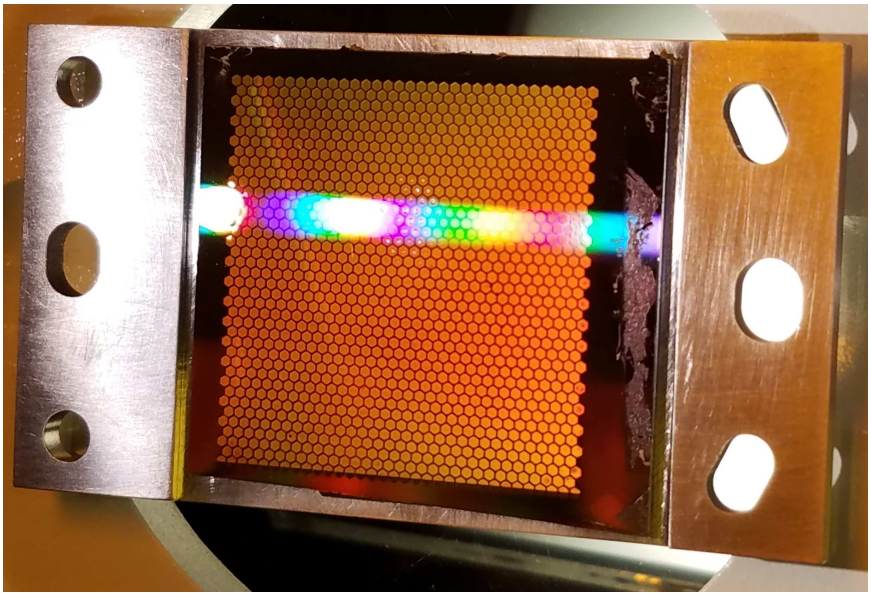

Figure 8. CAT grating X11, mounted to a titanium flexure frame. Only the 1 mm-size L2 hexagons are discernible. Visible light from a fiber is diffracted by the L1 mesh. The hexagons span an area of $\sim 32 \times 32$ mm^2.

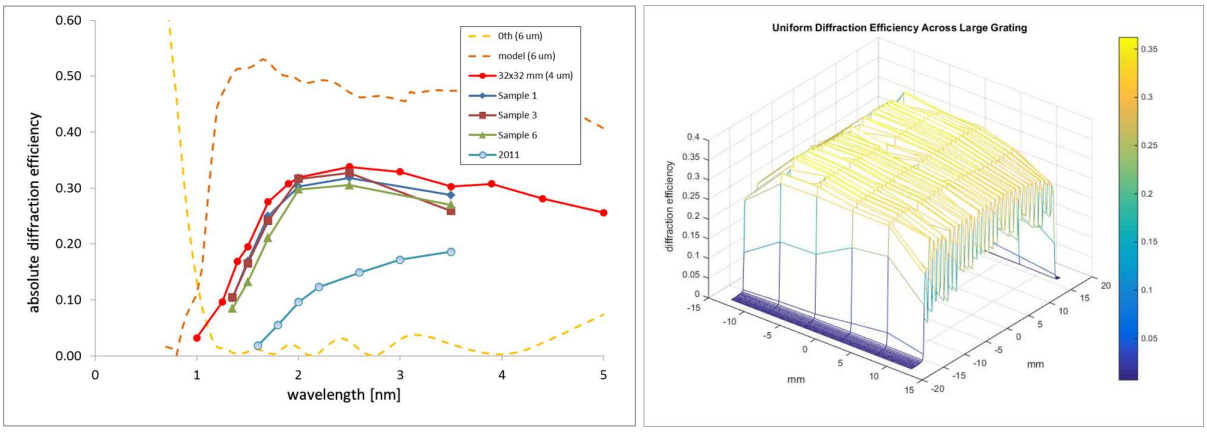

Figure 9. Left: Absolute diffraction efficiency (sum of orders near blaze, including L1 absorption) for grating X10 as a function of wavelength (red curve). Other samples were smaller gratings from previous years.[23] "Model" is the theoretical efficiency for 6 μm deep gratings (L1 absorption included) and shows the potential gains from deeper gratings. Right: Sum of absolute diffraction efficiencies from orders 3-8 near blaze at $\lambda = 2.5$ nm. The dips are due to partial blockage of the synchrotron beam by the hexagonal L2 mesh.

exceeds 30% across most of the grating surface. Sharp dips are due to partial blockage by the L2 mesh. Other large gratings have not yet been tested for efficiency, but based on experience with optical and scanning electron microscope imaging their performance is expected to be at a similar level as X10.

11. ROLL ALIGNMENT OF CAT GRATINGS IN AIR

Transmission gratings have relaxed alignment tolerances, but the dispersion axes of an array of gratings must still be aligned well enough to each other to take full advantage of the optical design to obtain the highest reasonably achievable resolving power. Grating roll (rotation about the grating normal) determines the direction of the dispersion axis and has the tightest alignment tolerance for Arcus at 5 arcmin. Grating pitch and yaw can be measured with reflected beams of visible light, but roll cannot, since for a 200 nm-period grating only the reflected and transmitted 0^{th} orders exist. Using x rays for alignment generally is much more time-consuming and expensive than using visible light and would require alignment under vacuum.

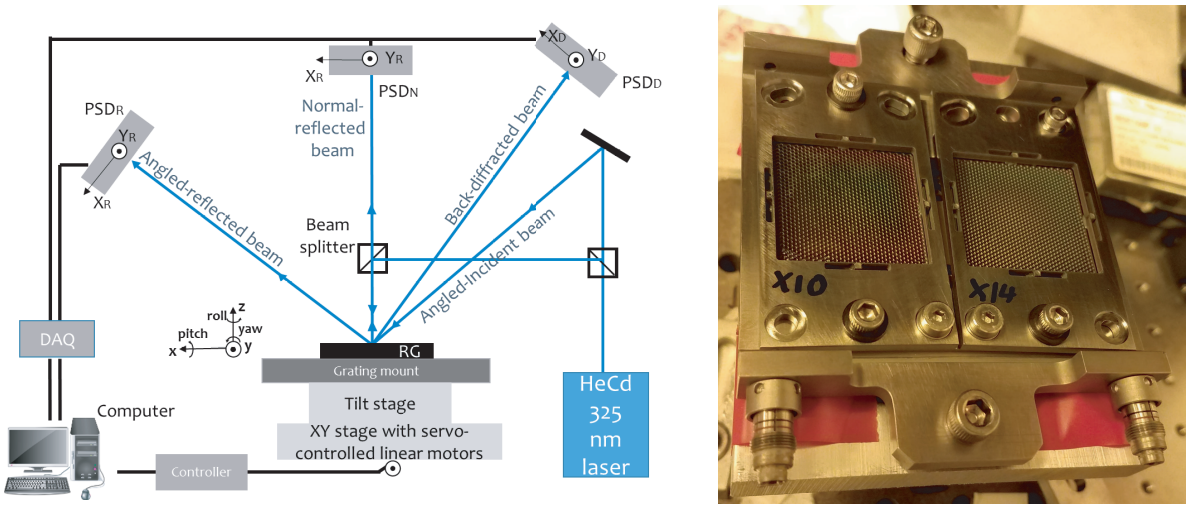

Figure 10. Left: Schematic of the roll-alignment setup using reflection and back-diffraction of UV light. This tool can also be used for precise grating period mapping and is described in detail by Song et al.[31] Right: Picture of gratings X10 and X14, glued onto Ti flexure frames, which are fastened to an alignment plate after roll alignment. The gratings are shown with the hexagonal L2 mesh facing upwards.

We have developed an alignment technique using UV laser light, based on the period measurement approach used for the Chandra HETG gratings.[30] It simultaneously measures angles of reflection and back-diffraction using a 325 nm-wavelength laser (see Fig. 10).

We epoxy-bonded the large gratings X10 and X14 to titanium flexure frames in four spots each. The frames carrying the gratings were then mounted - nominally in the same plane - to an alignment plate designed to allow for fine roll angle adjustment between the two gratings. The resulting grating alignment assembly was scanned (nominally) parallel to the grating surface, such that the laser beam incident at an angle of ~ 60 degrees from normal scanned a distance of 15 mm across the middle of each grating in a straight line. The roll angle for each grating was taken as the average value along the scanned path. After measuring both roll angles, the X14 roll angle was then adjusted via a micrometer, and the measurement was repeated. After achieving 3.4 ± 1.1 arcmin of roll angle difference $\Delta\rho$ between the gratings, fixture screws were carefully tightened, and $\Delta\rho$ was re-measured and found to be 0.08 ± 1.1 arcmin.

Details of the measurement setup, procedure, and data analysis are described in a separate paper.[31] The plate with the two gratings was then carefully packed and taken to the PANTER x-ray test facility in Germany for further measurements.

12. X-RAY MEASUREMENTS OF ALIGNED CAT GRATINGS

The PANTER x-ray test facility[32] of the Max-Planck Institute for Extraterrestrial Physics is qualitatively similar to the SLF. An electron bombardment source emits x rays into a 120 m long vacuum tube which merges into a 12 m long, 3.5 m diameter chamber. Near the end of the chamber is the TROPIC x-ray CCD camera (75 μm pixels),[35] mounted to an xyz linear translation stage stack. The same SPO modules that were used at the SLF had been realigned at the BESSY II synchrotron into an XOU (XOU-0038B) before being sent to PANTER for our measurements. The XOU was mounted to a hexapod with its node 13.283 m from the detector, and the grating alignment assembly was mounted to a second hexapod, with the gratings 198 mm downstream from the XOU node. A single aperture plate with xy translation was available and placed 229 mm upstream of the XOU node (see Fig. 11). The available apertures were 100% (66×15.5 mm^2), 64% (42×15.5 mm^2), 48% (32×15.5 mm^2) and 5% (3×15.5 mm^2). In order to measure roll alignment we observed the 10$^{\text{th}}$ order Mg K$_\alpha$ peak, alternatively selecting X10 and X14 with the 48% mask, while blocking the azimuthally outermost 3 mm of the SPO. From the difference in the location of the peaks the roll angle between the two gratings was determined to

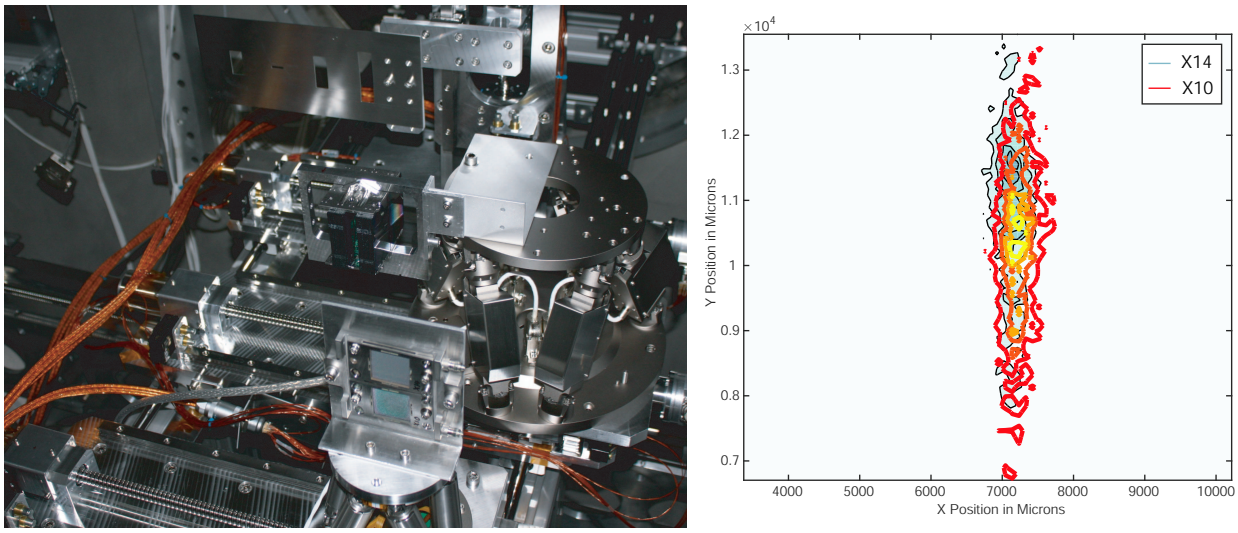

Figure 11. Left: Measurement setup at the PANTER x-ray test facility. In the front is the grating alignment assembly (on top of a small hexapod), behind it the XOU (suspended from a large hexapod), and in the back is the aperture plate. During measurement both XOU and gratings are positioned farther to the left. Right: Composite image of 10^{th} order Mg K_α peak contour plots from X10 and X11. The peak from X10 is shifted down by about 9 pixels (675 μm) relative to the peak from X14, corresponding to a rotation of 3.6 arcmin around 0^{th} order.

be 3.6 ± 1.2 arcmin, which is different from the value deduced from the last UV measurement and outside the estimated range of uncertainty, but close to the value measured before the last tightening of the fixture screws.

After the x-ray campaign at PANTER the grating alignment assembly was returned to MIT, the UV measurement was repeated, and $\Delta\rho$ was found to be 3.3 ± 1.1 arcmin. It is conceivable that stress buildup during the last tightening was released between the last pre-x-ray UV measurement and the x-ray tests, or that thermal effects allowed for a change in $\Delta\rho$. For future tests we intend to improve upon the design of the alignment assembly. Nevertheless, we believe that as an initial proof-of-principle our tests have shown that the UV alignment method is sufficiently precise to align CAT gratings to each other within the tolerances required for Arcus. No matter the actual cause, without permanent fixation (e.g. epoxy bonding) the grating frames can move with respect to each other. In an actual flight mission the frames would be permanently bonded in place to prevent movement after alignment.

We also measured diffraction peaks from the simultaneous illumination of both gratings, using the 64% mask. These data, together with diffraction peaks from the individual gratings, are currently being analyzed to extract resolving power.

13. CAT GRATING SPECTROMETER FOR LYNX

The science cases for Lynx are currently being assembled.[12] Several of the science cases are ideally addressed by a large effective area, high spectral resolving power soft x-ray grating spectrometer. Examples are characterization of the state of gas and diffuse baryons in galactic halos and the Milky Way halo, AGN winds (in combination with a microcalorimeter), and accretion onto young stars. Studies of similar CAT grating spectrometers have been performed before[11,25,33,34] and showed that such an instrument with the required performance can very feasibly be built in a Lynx-relevant time frame. We are currently revisiting the design with the most recent science questions and technology developments in mind. Fig. 12 shows an example projected effective area curve if a 3 m-diameter mirror assembly were fully covered with CAT grating arrays. In this example a coverage of only 63% of the telescope aperture with CAT gratings would provide 4000 cm^2 effective area at 0.3 keV. We are also studying limits on resolving power due to aberrations in the optical design that might arise when telescope

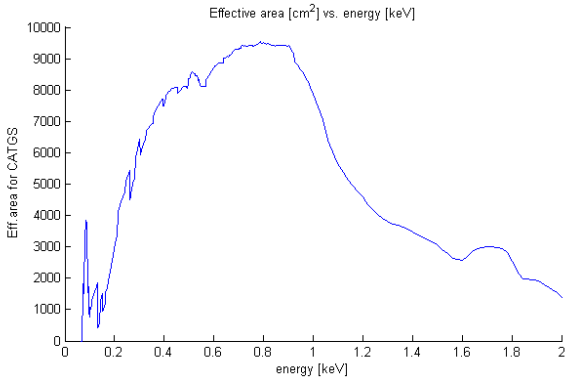

Figure 12. Example model prediction of effective area for dispersed x rays collected by a readout array as a function of energy. Full coverage of an example 3 m diameter mirror assembly for a 10 m focal length telescope is assumed.

coverage is increased relative to previous models - which predicted $R > 20,000$[33] - to see at which point multiple detector arrays might be required.

14. DISCUSSION

CAT gratings have been tested in combination with focusing SPOs to estimate their performance in an Arcus-like setup. Measuring resolving power $\lambda/\Delta\lambda$ of a grating spectrometer is difficult with a source spectrum that is broad compared to $\Delta\lambda$. Thus the narrow Al and Mg K_α lines ($\lambda/\Delta\lambda$ ~3450) are the most suitable sources in the soft x-ray band. For the above measurements at the SLF we were geometrically restricted in angle and could not reach the Arcus design incidence angle of 1.9 deg. (or blaze angle of 3.8 deg). Based on the measured LSF of the direct beam from the XOU one would expect to obtain in the best case R = 3400 and 3600 at 9^{th} order Al-K and 8^{th} order Mg-K, respectively. The lower values we obtained were mainly due to misalignment between the L1 mesh dispersion axis and the long direction of the optic PSF. Data analysis showed that with proper alignment we would achieve $R = 3000 - 3400$. Resolving power in these measurements is also reduced due to the finite source size. Taking its contribution into account and extrapolating to the Arcus blaze angles one predicts $R = 6900 - 7500$ with the tested XOU and CAT grating combination for illumination with a point source. Further removing the contribution from the optic LSF the gratings are compatible with R in the range of 10,000 to 16,000, similar to previous measurements.[7] The Arcus optical design error budget calls for a 2 arcsec (FWHM) optic LSF and R being limited to 6000 by the gratings alone.[9] Our spectrometer prototype exceeds these requirements.

Misalignment of the L1 dispersion axis was a complication in this demonstration with a single XOU. We do not expect this to be a problem for Arcus for two reasons: First, the Arcus effective area is dominated by contributions from diffraction orders at larger diffraction angles and orders than tested here. Spectral features can be more easily resolved in higher orders m, but non-negligible L1 diffraction will remain limited to small values of $n \sim \pm 1, 2$ and contribute less potential broadening on a relative scale. Second, the combined LSF from a whole Arcus grating petal will be much broader than the measured LSF in this work, and any potential broadening from L1 misalignment will thus be a much smaller fraction of the total FWHM. In addition, the relative orientation between CAT grating bars and the L1 mesh can be made more precise with straightforward alignment steps during patterning, if necessary.

Two frame-mounted CAT gratings were environmentally tested to General Environmental Verification Standard (GSFC-STD-7000) levels. The gratings survived visibly intact, and measurements of resolving power and diffraction efficiency showed no decline in performance. Multiple three-times-larger gratings have been fabricated with high yield. The only large grating systematically x-ray tested so far has homogeneous diffraction efficiency with slight improvement over previous results. These results confirm that we have a mature fabrication process for large-area gratings. With the lessons learned over the years we expect that we can increase the grating size to within 10 mm of the edge of a 100 mm wafer with our current tools. Larger gratings will have to be environmentally tested again to ensure that larger form factors also will withstand launch vibrations.

CAT grating throughput can simply be increased through the use of more narrow L2 structures, which currently block almost 20% of the grating area. However, there might be a trade-off with regards to robustness during fabrication and launch. This is an area of research where we have not done any optimization yet. CAT grating efficiency is typically within 80-100% of what models based on the achieved structures predict.[14,16,23] Fabricating deeper (e.g. 6 μm deep 200 nm period) gratings thus promises significant gains in efficiency, as shown in Fig. 9. While we have successfully performed the DRIE step for such geometries, the comprehensive CAT grating fabrication process has not yet been attempted.

We have demonstrated that we can align two CAT gratings in roll to better than 5 armin with a UV laser technique. According to more recent ray tracing this tolerance for Arcus might be even more relaxed than 5 arcmin.[26]

The resolving power for a Rowland torus CAT grating spectrometer is limited mainly by four quantities: The LSF of the focusing optics, the blaze angle, aberrations inherent in the optical design and deviations of flat gratings from the curved torus surface, and period variations in the gratings themselves. Measuring the latter in air eliminates the need to determine the resolving power of each grating in a large x-ray facility. The UV laser technique we used for roll alignment is currently being adapted for this task.[31]

Deviations from the Rowland torus could be minimized by using many small gratings - which would increase cost - or by bending large flat gratings in the plane of dispersion. Initial bending tests with a CAT grating (performed in the context of a soft x-ray polarimetry sounding rocket experiment)[36] make the latter approach appear to be quite feasible.[37] This ability could have a significant positive impact on the performance of a CAT grating spectrometer for both Arcus and Lynx.

Finally, the MIT polarimetry beamline was recently reconfigured for optimized x-ray testing of CAT gratings.[37] This allows for rapid in-house evaluation of gratings before major external measurement campaigns.

15. SUMMARY

CAT grating technology has reached a high level of maturity and can be incorporated into a flight mission. We have demonstrated that CAT gratings paired with SPOs perform in accordance with expectations and exceed requirements for the Arcus mission in terms of efficiency and resolving power. The gratings have survived environmental testing without damage. Current grating size exceeds the baseline Arcus design of 23×28 mm^2, and we can align gratings in roll with better precision than required.

ACKNOWLEDGMENTS

We gratefully acknowledge support from E. Gullikson (ALS), help with figures from T. Ferry (MIT), and facilities support from the Nanostructures Laboratory and the Microsystems Technology Laboratories (both at MIT). We appreciate support from Marshall Space Flight Center for work done at the SLF. A part of this work used resources of the Advanced Light Source, which is a DOE Office of Science User Facility under contract no. DE-AC02-05CH11231. Part of the work performed at PANTER has been supported by the European Unions Horizon 2020 Programme under the AHEAD project (grant agreement n. 654215). This work was supported by NASA grants NNX15AC43G and NNX17AG43G, SAO, and the MIT Kavli Institute for Astrophysics and Space Research.

REFERENCES

[1] Brenneman, L. W., *et al.*, "The evolution of structure and feedback with Arcus," *Proc. SPIE* **9905**, 99054P (2016).

[2] "New Worlds, New Horizons in Astronomy and Astrophysics," National Research Council, http://www.nap.edu/catalog.php?record_id=12951 (2010).

[3] "Enduring Quests, Daring Visions," NASA 2013 Astrophysics Roadmap, http://science.nasa.gov/media/medialibrary/2013/12/20/secure-Astrophysics_Roadmap_2013.pdf

[4] Canizares, C. R. *et al.*, "The Chandra high-energy transmission grating: Design, fabrication, ground calibration, and 5 years in flight," *PASP* **117**, 1144-1171 (2005).

[5] den Herder, J. W. *et al.*, "The reflection grating spectrometer on board XMM-Newton," *Astr. & Astroph.* **365**, L7-L17 (2001).

[6] NASA Astrophysics Division Physics of the Cosmos Program Annual Technology Report, http://pcos.gsfc.nasa.gov/technology/

[7] Heilmann, R. K., Bruccoleri, A. R., Kolodziejczak, J., Gaskin, J. A., ODell, S. L., Bhatia, R., and Schattenburg, M. L., "Critical-Angle X-ray Transmission Grating Spectrometer with Extended Bandpass and Resolving Power $> 10,000$," *Proc. SPIE* **9905**, 99051X (2016).

[8] Smith, R. K. *et al.*, "Arcus: The X-ray Grating Spectrometer Explorer," *Proc. SPIE* **9905**, 99054M (2016).

[9] Smith, R. K. *et al.*, "Arcus: Exploring the Formation and Evolution of Clusters, Galaxies, and Stars," *Proc. SPIE* **10397**, paper 27, to be published (2017).

[10] Collon, M. J., Ackermann, M., Günther, R., Chatbi, A., Vacanti, G., Vervest, M., Yanson, A., Beijersbergen, M. W., Bavdaz, M., Wille, E., Haneveld, J., Olde Riekerink, M., Koelewijn, A., van Baren, C., Müller, P., Krumrey, M., Burwitz, V., Sironi, G., and Ghigo, M., "Making the Athena optics using silicon pore optics," *Proc. SPIE* **9144**, 91442G (2014); Collon, M. J. *et al.*, "Development of Athena mirror modules," *Proc. SPIE* **10399**, paper 11, to be published (2017).

[11] Gaskin, J. *et al.*, "The X-ray Surveyor Mission: A Concept Study," *Proc. SPIE* **9601**, 96010J (2015).

[12] Gaskin, J. A., "Lynx mission concept status," *Proc. SPIE* **10397**, paper 29, to be published (2017).

[13] Heilmann, R. K. *et al.*, "Critical-angle transmission gratings for high resolution, large area soft x-ray spectroscopy," Response to NASA solicitation NNH11ZDA018L, http://pcos.gsfc.nasa.gov/studies/rfi/Heilmann-Ralf-RFINNH11ZDA018L.pdf (2011).

[14] Heilmann, R. K., Ahn, M., Gullikson, E. M. and Schattenburg, M. L., "Blazed high-efficiency x-ray diffraction via transmission through arrays of nanometer-scale mirrors," *Opt. Express* **16**, 8658-8669 (2008).

[15] Heilmann, R. K., Ahn, M. and Schattenburg, M. L., "Fabrication and performance of blazed transmission gratings for x-ray astronomy," *Proc. SPIE* **7011**, 701106 (2008).

[16] Heilmann, R. K., Ahn, M., Bruccoleri, A., Chang, C.-H., Gullikson, E. M., Mukherjee, P. and Schattenburg, M. L., "Diffraction efficiency of 200 nm period critical-angle transmission gratings in the soft x-ray and extreme ultraviolet wavelength bands," *Appl. Opt.* **50**, 1364-1373 (2011).

[17] Ahn, M., Heilmann, R. K. and Schattenburg, M. L., "Fabrication of ultrahigh aspect ratio freestanding gratings on silicon-on-insulator wafers," *J. Vac. Sci. Technol. B* **25**, 2593-2597 (2007).

[18] Ahn, M., Heilmann, R. K. and Schattenburg, M. L., "Fabrication of 200 nm-period blazed transmission gratings on silicon-on-insulator wafers," *J. Vac. Sci. Technol. B* **26**, 2179-2182 (2008).

[19] Mukherjee, P., Bruccoleri, A., Heilmann, R. K., Schattenburg, M. L., Kaplan, A. F. and Guo, L. J.,"Plasma etch fabrication of 60:1 aspect ratio silicon nanogratings on 200 nm pitch," *J. Vac. Sci. Technol. B* **28**, C6P70-5 (2010).

[20] Bruccoleri, A., Mukherjee, P., Heilmann, R. K., Yam, J. and Schattenburg, M. L., "Fabrication of nanoscale, high throughput, high aspect ratio freestanding gratings," *J. Vac. Sci. Technol. B* **30**, 06FF03 (2012).

[21] Bruccoleri, A. R., Guan, D., Vargo, S., DiPiazza, F., Heilmann, R. K. and Schattenburg, M. L., "Nanofabrication advances for high efficiency critical-angle transmission gratings," *Proc. SPIE* **8861**, 886119 (2013).

[22] Bruccoleri, A. R., Guan, D., Mukherjee, P., Heilmann, R. K., Schattenburg, M. L. and Vargo, S., "Potassium hydroxide polishing of nanoscale deep reactive-ion etched ultra-high aspect ratio gratings," *J. Vac. Sci. Technol. B* **31**, 06FF02 (2013).

[23] Heilmann, R. K., Bruccoleri, A. R., and Schattenburg, M. L., "High-efficiency blazed transmission gratings for high-resolution soft x-ray spectroscopy," *Proc. SPIE* **9603**, 960314 (2015).

[24] Bruccoleri, A. R., Heilmann, R. K., and Schattenburg, M. L., "Fabrication Process for 200 nm-Pitch Polished Freestanding Ultra-High Aspect Ratio Gratings," *J. Vac. Sci. Technol. B* **34**, 06KD02 (2016).

[25] Heilmann, R. K. *et al.*, "Critical-angle transmission grating spectrometer for high-resolution soft x-ray spectroscopy on the International X-Ray Observatory," *Proc. SPIE* **7732**, 77321J (2010).

[26] Günther, H. M. *et al.* "Performance of a double tilted-Rowland-spectrometer on Arcus," *Proc. SPIE* **10397**, paper 26, to be published (2017).

[27] Cash, W.,"X-ray optics: a technique for high-resolution imaging," *Appl. Opt.* **26**, 2915 (1987).

[28] McEntaffer, R. *et al.*, "First results from a next-generation off-plane X-ray diffraction grating," *Exp. Astron.* **36**, 389 (2013).
[29] Schweppe, J., Deslattes, R. D., Mooney, T., Powell, C. J., "Accurate measurement of Mg and Al K$\alpha_{1,2}$ X-ray energy profiles," *J. Electron Spectrosc. Relat. Phenom.* **61**, 463 (1994).
[30] Dewey, D., Humphries, D. N., McLean, G. Y. and Moschella, D. A., "Laboratory calibration of x-ray transmission diffraction gratings," *Proc. SPIE* **2280**, 257 (1994).
[31] Song, J., Heilmann, R. K., Bruccoleri, A. R., Hertz, E., and Schattenburg, M. L., "Scanning laser reflection tool for alignment and period measurement of critical-angle transmission gratings," *Proc. SPIE* **10399**, paper 40, to be published (2017).
[32] Burwitz, V. *et al.*, "In focus measurements of IXO type optics using the new PANTER x-ray test facility extension". *Proc. SPIE* **8861**, 88611J (2013).
[33] Günther, H. M., Bautz, M. W., Heilmann, R. K., Huenemoerder, D. P., Marshall, H. L., Nowak, M. A., and Schulz, N. S., "Ray-tracing critical-angle transmission gratings for the X-ray Surveyor and Explorer-size missions," *Proc. SPIE* **9905**, 990556 (2016).
[34] Vikhlinin, A. *et al.*, "SMART-X: Square meter arcsecond resolution x-ray telescope, *Proc. SPIE* **8443**, 844316 (2012).
[35] Meidinger, N. *et al.*, "CCD detectors for spectroscopy and imaging of x-rays with the eROSITA space telescope," *Proc. SPIE* **7435** 743502 (2009).
[36] Marshall, H. L. *et al.*, "The rocket experiment demonstration of a soft x-ray polarimeter," *Proc. SPIE* **10397**, paper 21, to be published (2017).
[37] Heine, S. *et al.*, "Laboratory progress in soft x-ray polarimetry," *Proc. SPIE* **10399**, paper 41, to be published (2017).